

Article

Coil Parameter Analysis for Inductively Coupled Wireless Charging for Electric Vehicles

Viswanath Chakibanda and Venkata Lakshmi Narayana Komanapalli * 

School of Electrical Engineering, Vellore Institute of Technology, Vellore 632014, Tamil Nadu, India; chakibanda.viswanath2020@vitstudent.ac.in

* Correspondence: vlnarayana.k@vit.ac.in

Abstract: Wireless charging (WC) has gained popularity for the charging of electric vehicles in recent years of research, particularly dynamic wireless charging systems (DWCSs). Among the different topologies of DWCSs, this paper focuses on an inductively coupled wireless charging system (ICWCS). In this ICWCS, double-D (DD) coils create horizontal and vertical flux components between different pad configurations, which show optimal features in contrast to circular pad coils. In this work, the three-dimensional (3D) finite element technique (FEM) is used to establish the proposed design to observe the coupling coefficient, while the system design's performance is evaluated using a circuit simulator. In the simulation, the proposed DD coil configuration is used for both the transmitter and receiver sides. It provides the maximum coupling coefficient and efficiency at perfect alignment when using an in-between air gap of 166 mm and six I-type ferrite bars on the transmitter side and five I-type ferrite bars on the receiver side. The coupling coefficient and system parameters, such as power and efficiency, are considered for different misalignments in the proposed configuration. The results of this work satisfy the Society of Automotive Engineers (SAE) J2954 Class 3 criteria. The best results obtained are on account of optimizing the ferrite core, which is achieved by varying its length and width. While varying the ferrite core's dimensions, 0.2451, as the optimal k value, is obtained at the effective width and length of 57.5 mm and 400 mm, respectively. The simulation results of the Ansys Maxwell 3D software prove the feasibility of the proposed structure.



Citation: Chakibanda, V.; Komanapalli, V.L.N. Coil Parameter Analysis for Inductively Coupled Wireless Charging for Electric Vehicles. *Vehicles* **2024**, *6*, 468–483. <https://doi.org/10.3390/vehicles6010021>

Academic Editors: José González-González, Alicia Triviño-Cabrera and Binh Vu

Received: 23 December 2023
Revised: 17 February 2024
Accepted: 22 February 2024
Published: 28 February 2024



Copyright: © 2024 by the authors. Licensee MDPI, Basel, Switzerland. This article is an open access article distributed under the terms and conditions of the Creative Commons Attribution (CC BY) license (<https://creativecommons.org/licenses/by/4.0/>).

Keywords: coupling coefficient; double-d coils; electric vehicle; wireless charging; dynamic wireless charging system

1. Introduction

Researchers in the electric vehicle (EV) domain have suggested that, among present-day commercial technological adaptations, wireless charging is one of the most effective ways to preserve the environment. Further, in recent years, WC has gained popularity among the various charging methods for charging EVs. In WC, mutual induction, as proposed by Sir Nikola Tesla, involves the generation of an induced electromotive force (emf) in the second coil, termed the receiver coil. This induced emf enables the conversion of electrical energy by utilizing a specified current in the first coil, referred to as the transmitter coil [1]. Today's wireless charging and power transmission technologies are a result of Tesla's revolutionary work in these fields. The development of wireless charging for electric vehicles leads to improved user comfort, eliminates physical connectors, addresses concerns about cable wear, and encourages a smooth and automated charging experience. Also, some studies have focused on the selection of a motor for EVs and complete vehicle dynamics to obtain further optimal results [2].

Studies have revealed that, compared to capacitive charging, inductive charging has a significantly greater efficiency and power density. The report [3] outlines industry-standard research and developments related to DWCSs, particularly for inductive power transfer

(IPT). The dimensions of coupling coils have a substantial impact on the inductive parameters [4]. The authors introduced a design methodology for a serial–serial (SS) wireless system, detailing the process of determining optimal pad dimensions to facilitate power transfer to the EV battery [5]. Many academics and industry experts are focused on transferring maximum power to the receiving pad, which boosts an EV's efficiency in dynamic conditions. To improve coupling between transmitter and receiver coils, several magnetic couplers have been suggested. According to some studies, the percentage efficiency, especially for inductive power transmission, can exceed 90% [6]. Also, in the study [7], the plausible cost savings gained were estimated via the reduced carbon footprint of passenger vehicle mobility, with the widespread adoption of dynamic wireless power transfer on roads expected in coming decades. In [8], the authors tried to show the practical feasibility of DWCSs constrained to the health/state of the battery and the lesser availability of charging lanes.

1.1. Outline of WPT System for EVs

Figure 1 outlines the steps in an EV wireless charging system (WCS). First, on the transmitter side, AC is converted to DC using an adaptive front end (AFE). Then, on the same side, the inverter is connected further and transforms into high-frequency AC for efficient power transfer. Then, a high-frequency transformer (HFT) is connected to this inverter in order to make the topology failsafe. This HFT generates an alternating magnetic field, as per Ampere's law. A reactive power compensation network, for smooth operation, links the HFT and transmitting coil (Tx). The high-frequency magnetic field is transferred to the receiving coil (Rx) through its turns and structure. Finally, a reactive power compensation network qualifies the resonant state to boost efficiency at the receiver side.

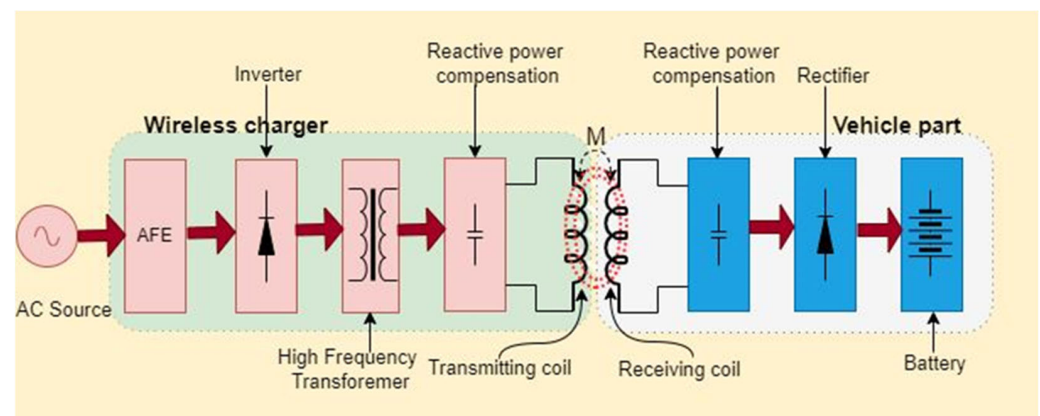


Figure 1. Schematic of the wireless charging system for EVs.

Though the discussion in this work is limited to coil structure, there are other components that play crucial roles in designing a WPT system for an EV that employs these coil structures, as shown in Figure 1. In addition to these components, operational factors, like addressing alignment challenges, adapting to dynamic charging conditions, implementing foreign object detection, managing temperature, taking into account frequency of use, ensuring stable grid connectivity, user-friendly interfaces, regulatory compliance, infrastructure integration, and robust network connectivity, are all critical aspects of optimizing the WPT system for an EV.

1.2. Wireless Charging Power Pad

An essential element of the resonant inductive power transfer system is the magnetic coupler. A magnetic coupler comprises the transmitter, receiver, and shielding frame coils. Power is delivered between the transmitter and receiver coils via air, and shielding controls flux scattering.

In [6], the authors reviewed the critical characteristics and design elements of the polarized and nonpolarized power pad architectures utilized in IPT systems. In [9], the authors used multi-objective optimization to compare several magnetic couplers for inductive-based EV charging. In [10], authors compared four coupler topologies with respect to the coupling factor under different displacement circumstances to determine the best coupler design. Through a comparison of flux pathways, the authors in [11] have investigated the basic limitations of currently available inductive couplers and analytically suggested better coupler variations. Figure 2a,b show an expanded view and top view of a wireless charging power pad. The protecting cover (plastic cover) protects the power pad; the coil and coil former generate a magnetic field; ferrite is used to align the magnetic field; the aluminum plate holds the power pad; and the aluminum backing plate holds the complete system. Aluminum is utilized to lighten it.

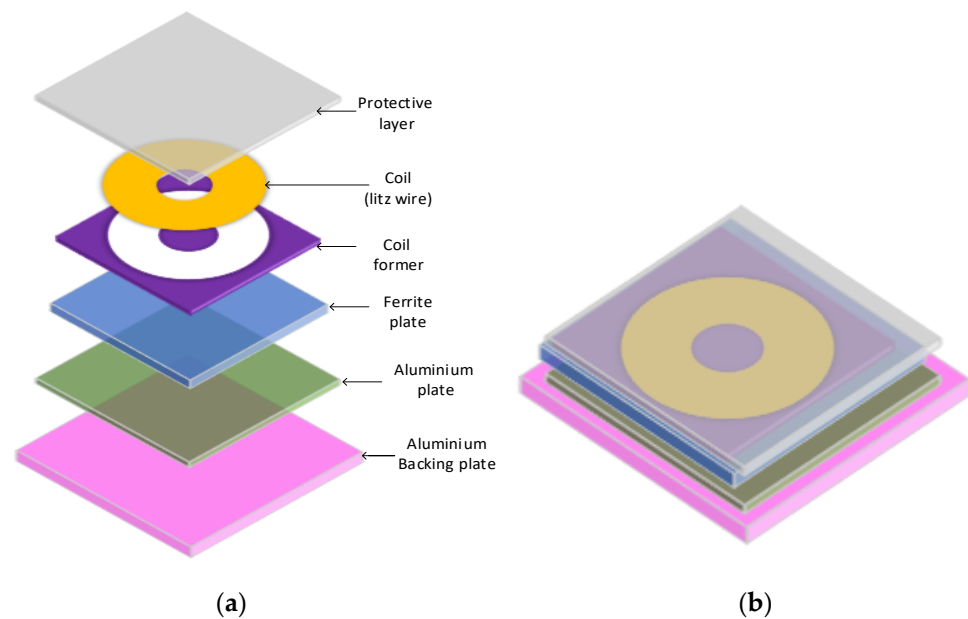


Figure 2. Wireless charging power pad [6]: (a) Expanded view; (b) Top view.

In the WPT system, assessing the self and mutual inductance characteristics is pivotal in analyzing the magnetic properties of power pad coil configurations. Various shapes have been incorporated in transformer design to enhance power transfer efficiency, intensifying the intricacies of parameter calculations. Fortunately, leveraging finite element analysis can potentially streamline the resolution of these challenges [9]. In [12], a new analytical calculation of the mutual inductance between the coaxial spiral rectangular coils is derived to maximize the design of the transmitting coil under a condition constraint on space, which limits the size of the received coil. Further, the article [13] analyzes data for the estimation of the equivalent mutual inductance of permanent magnets and massive coils. This study provides results suitable for further optimization as well.

Mutual inductance is calculated by employing 3D FEM at various possible misalignments, which is time-demanding [14]. Analytical models are frequently used to save computation time. In [15], the authors propose a 3D analytical approach for calculating the mutual inductance of various rectangular coil misalignments. When compared to the FEM model, the analytical models are built with approximations, which results in poor accuracy in the conclusions. However, because analytical models require less time to compute, they can be employed to perform initial system sizing. In [16], an analytical approach using the Biot–Savart law is proposed for determining the mutual inductance between two air-core square coils. In [17], utilizing both the FEM theory and experimental data, the magnetic core’s physical parameters are optimized, and the structure of DD coils is fine-tuned to achieve a significant coupling coefficient. This optimization allows the development of

a cost-effective WPT system with substantial increase in efficiency. Additionally, a novel approach is presented for optimizing the stray parameters of DD coils, taking into account the unique flux path. The mutual inductance of different geometrical coils (rectangular and square) is studied, as reported in [12,13,15,16]. These reported studies also investigated mutual inductance in the case of vertical and horizontal misalignments and that of other plausible misalignments—angular, planar, and their combination with horizontal, as well.

There are various DWCS topologies. In [18], regarding DWCS, the authors explore the utilization of the two predominant coil configurations in IPT systems at the simulation level. This study has involved two distinct pad types—namely, the distributed dynamic pad (DDP) and rectangular pads positioned on the side of the car. The assessment has considered the DDP as a universal transmitter and repeated the process with the rectangular pad as the general transmitter, evaluating the system's performance under varying configurations. In [19], the impact of square-coil ferrite cores on the coupling coefficient is described as about 41.8% greater than that of the DD coil, where the air gap is 70 mm and the primary and secondary coils both have equal area. Moreover, when the X-axis misalignment is up to 150 mm, the DD coil's anti-offset range is larger [19]. In [20], the anti-misalignment's mitigation ability is compared between the circular DD coils and rectangular DD coils. In [20,21], these papers delve specifically into the intricacies of ICWCS. This ICWCS focuses on exploring the efficacy of DD coils compared to circular pad and rectangular pad coils, as they generate both horizontal and vertical flux components, exhibiting optimal features across various pad configurations. The afore-mentioned studies and [6,9,22] point out that the DD coil is advantageous for DWCS because of the following: it is relatively more tolerant to misalignment than circular and rectangular coils, has a lower flux leakage, and exhibits a higher coupling coefficient. Hence, these coils become more efficient and effective in power transfer. In [23], the authors have proposed a multi-objective optimization method for a primary DD pad in IPT systems, using a parametric sweep analysis to identify crucial design parameters. They employed the nondominated sorting genetic algorithm II to optimize the pad's structure, prioritizing a high coupling coefficient while minimizing the worst-case stray leakage magnetic field. In [24], the authors introduced a core design and optimization strategy for DD coil topologies, which considers a unique flux path. This results in a significantly reduced core loss through the implementation of optimized thickness and core structure. In [25], the authors examined the implementation of a full-ferrite DD pad and proposed a cost-effective solution for IPT systems in EV charging by integrating ferrite-based soft magnetic composites (SMCs). The IPT pad design outlined in this study explores the substitution or elimination of ferrite with SMCs to enhance system affordability and mechanical durability. Figure 3a shows the polarized DD coil with ferrite bars, and Figure 3b shows the coil with ferrite bars and an aluminum plate. Apart from the structure of coils, ferrite cores have a significant role to play in optimization. The research in [21] compares several ferrite topologies and the impact of parameter values on the magnetic coupling coefficient for a 13 mm rectangular coil on both sides. In the ferrite context, the authors designed them based on machine learning to establish a high coupling coefficient between the Tx and Rx coils [22].

Table 1 explores the inferences related to I-type ferrite bars with DD coil pads. The novelty of this article comprises the consideration of DD coils, six I-type ferrite bars on the transmitter side, and five I-type ferrite bars on the receiver side while simulating the proposed system. On the transmitter side, each of the ferrite bars is 600 mm × 52.5 mm × 8 mm, and on the receiver side, it is 540 mm × 52.5 mm × 8 mm in dimension. The gap between the ferrite bars is 22.5 mm on both sides. In addition to this, the following three cases are considered while optimizing the ferrite dimensions to achieve the highest k :

- Case 1: The length of the ferrite bars is varied at Tx, Rx, and both Tx and Rx by maintaining a constant ferrite width for the optimal value of length to maximize the value of ' k ';

- Case 2: The width of the ferrite bars is varied at Tx, Rx, and both Tx and Rx by maintaining a constant ferrite length for the optimal value of width to maximize the value of 'k';
- Case 3: Both the length and width of the ferrite bars are varied at Tx, Rx, and both Tx and Rx for the optimal values of length and width to maximize the value of 'k'.

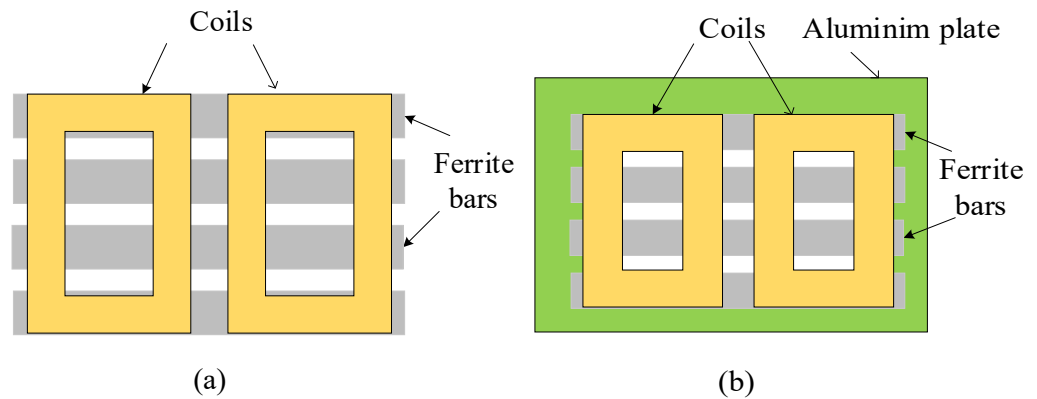


Figure 3. Polarized DD coil: (a) with ferrite bars; (b) with ferrite bars and aluminum plate.

Table 1. Inferences related to I-type ferrite bars with a DD coil pad.

Reference	Type of Coil Pad on Tx-Rx Sides	Type of Core on Tx-Rx Sides	Inference
[26]	Case 1: Both sides—Rectangular Case 2: Both sides—DD	Both sides—I-type ferrite bars	Objective: Comparing rectangular winding design to DD winding in IPT coils with the same outer dimensions, the main merits and demerits are discussed using Pareto analysis. Shortfall: The effect of the change in dimensions of I-type ferrite bars is not considered.
[9]	Case 1: Both sides—Circular Case 2: Both sides—Rectangular Case 3: Both sides—DD Case 4: Tx side—DD and Rx side—DDQ	Both sides—I-type ferrite bars	Objective: The authors presented a multi-objective optimization framework to evaluate the performance of four coupler topologies. Presented merits, demerits, and trade-offs in key parameters such as efficiency, power density, misalignment tolerance, and stray field for all geometries. Shortfall: The effect of the change in dimensions of I-type ferrite bars is not considered.
[17]	Case 1: Both sides—DD	Both sides—I-type ferrite bars	Objective: Proposed optimization of the horizontal spacing of DD coils and the length of cores. Shortfall: On each side, six I-type ferrite bars are used and only the length of the ferrite bar is varied.
[23]	Case 1: Only on Tx side—DD	Only on Tx side—I-type ferrite bars	Objective: Introduced a multi-objective optimization method for I-type ferrite bars with a primary DD pad in inductive power transfer systems while considering four I-type ferrite bars and three I-type ferrite bars. With the utilization of nondominated sorting genetic algorithm II, the DD pad structure is optimized to achieve a high coupling coefficient and minimize worst-case stray leakage magnetic fields. Shortfall: Simultaneous variation in length and width is not considered. The length and width are varied individually only on the Tx side.

Table 1. Cont.

Reference	Type of Coil Pad on Tx-Rx Sides	Type of Core on Tx-Rx Sides	Inference
[27]	Case 1: Both sides—DD	Tx side—I-type ferrite Rx side—rectangular plate	Objective: Achieved the most effective mutual inductance value to obtain the maximum efficiency when the distance between ferrite bars is 15 mm. Shortfall: 25 I-type ferrite bars are used at the transmitter side, and only the gap between ferrite bars is varied.
Proposed	Case 1: Both sides—DD	Both sides—I-Type ferrite bars	Objective: In this study of DD coils, six I-type ferrite bars on the transmitter side and five I-type ferrite bars on the receiver side are considered for optimal design. Highlights: The length and width varied on the Tx and Rx sides, as well as simultaneously on both sides, to achieve the best coupling coefficient.

The structure of the proposed work begins with the design and development of the WCS's magnetic induction and the 3D modelling of the transmitting and receiving coils. Additionally, the efficiency of the proposed system is shown, which is aligned with the SAE J2954 Class 3 standard. Further, the efficiency of lateral and longitudinal misalignment is determined. Finally, ferrite structural optimization is followed by a conclusion.

2. Methodology and System Model

2.1. Methodology

As mentioned in Section 1.2 regarding the advantages of DD coils, the system design employs a 3D FEM for assessing the coupling coefficient, while its performance is rigorously examined using a circuit simulator. According to the simulation outcomes, the proposed DD coil configuration implemented on both the transmitter and receiver sides attains the maximum coupling coefficient (k_m) and efficiency at perfect alignment, maintaining an air gap of 166 mm. This optimal performance is achieved by strategically placing six I-type ferrite bars on the transmitter side and five on the receiver side. The results adhere to the SAE J2954 Class 3 criteria. The study further scrutinizes the coupling coefficient and system parameters, including power and efficiency, under different misalignments in the proposed configuration. The coupling coefficient is a measure of how well the magnetic field from the transmitter coil is coupled to the receiver coil in the WCS. It is a key parameter that affects the overall efficiency of power transfer. The coupling coefficient is inversely proportional to the square of the distance between the coils. As the vertical distance increases, the magnetic field strength between the coils decreases, leading to a lower coupling coefficient and vice-versa. However, the 'k' is directly proportional to efficiency, so as the distance between the coils increases, the efficiency decreases and vice-versa. The paramount focus of this research centers on the optimization of the ferrite core, achieved by varying its length and width while maintaining a thickness of 8 mm throughout the design analysis. The feasibility of the proposed structure is validated through simulation results obtained using Ansys Maxwell 3D software.

2.2. System Model: DD Coil Setup for ICWCS

Figure 4 depicts the design of the proposed DD coil setup for charging electric vehicles. The transmitter has two rectangular coils (DD coils) connected in series. Each coil has 15 turns side by side, a 7.4 mm diameter made up of copper, and the length and width of the internal rectangle are 200 mm and 52.6 mm, respectively. Six I-type ferrite bars are used on the transmitter side; each ferrite bar's dimensions are 600 mm × 52.5 mm × 8 mm, and the gap between ferrite bars is 22.5 mm. The receiver has two rectangular (DD coils) coils connected in series, having 13 turns side by side and a 7.4 mm diameter made up of copper.

The length and width of an internal rectangle are 150 mm and 52.6 mm, respectively. Five I-type ferrite bars are used on the receiver side; each ferrite bar’s dimensions are 540 mm × 52.5 mm × 8 mm, and the gap between ferrite bars is 22.5 mm. The vertical gap between the transmitter and receiver is 166 mm, which should comply with SAE standard J2954’s WPT/Z2 when the vertical gap Z is between 140 and 210 mm [28]. The relative permeability of the ferrite is 1000.

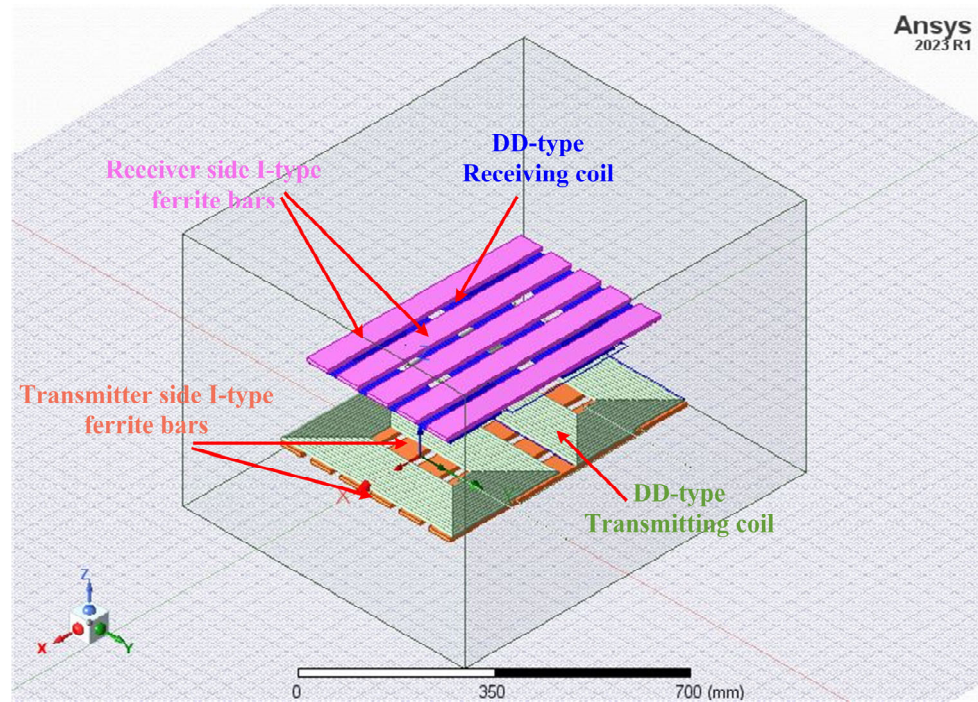


Figure 4. Isometric view of a perfectly aligned DD coil pad with an I-type ferrite core.

3. Analysis of the Proposed Structure

3.1. Performance of the ICWCS at Different Misalignments

As depicted in Figure 1, optimal efficiency is achieved when employing the basic series–series (SS) resonant compensation topology at the resonant angular frequency. For the circuit shown in Figure 5, load resistance can be calculated from Equations (2) and (3) to obtain the maximum efficiency and power, respectively.

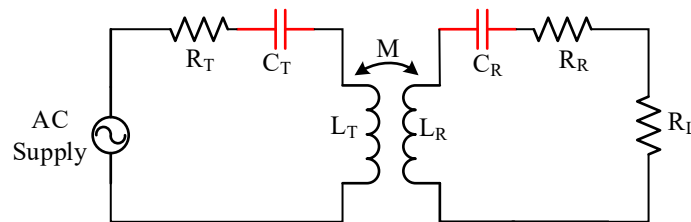


Figure 5. Basic series–series (SS) resonant compensation topology.

$$k = \frac{M}{\sqrt{L_T L_R}} \tag{1}$$

$$\eta = \frac{\omega^2 k^2 L_T L_R R_L}{[R_T(R_L + R_R) + \omega^2 k^2 L_T L_R](R_L + R_R)} \tag{2}$$

where $\omega = 2\pi f$.

For maximum efficiency, the optimal load resistance is determined using Equation (2), as

$$R_L = \sqrt{R_R^2 + \frac{\omega^2 k^2 L_T L_R R_R}{R_T}}$$

$$P = I_R^2 R_L = \frac{\omega^2 k^2 L_T L_R U_s}{[R_T(R_L + R_R) + \omega^2 k^2 L_T L_R]^2} R_L \tag{3}$$

For maximum power, the optimal load resistance is determined using Equation (3), as

$$R_L(P) = R_T R_R + \frac{\omega^2 k^2 L_T L_R R_R}{R_T}$$

$$f_{resonant} = \frac{1}{2\pi\sqrt{LC}} \tag{4}$$

Ansys Maxwell 3D and Simplorer are used in this design to show the current parameter of the WPT system. The Maxwell simulation results in a mutual inductance of 42.96 μH between Tx and Rx coils, and the self-inductances are 248.64 μH and 157.96 μH for Tx and Rx, respectively. These inductance values are exported to the Ansys Simplorer circuit which is an SS compensation topology, as shown in Figure 6. In this circuit, C1 and C2 are compensating capacitances at the transmitter and receiver sides, respectively. When the circuit resonates at 85 kHz, Equation (4) gives C1 and C2 as 16.4 nF and 27.5 nF, respectively. P1 and P2 measure the power at the source and load sides, respectively. Further, Figure 7 shows the graph of frequency versus efficiency, and denotes that at 85 kHz resonant frequency in the perfectly aligned case, 98.52% efficiency is achieved. Figure 8 describes that the output power is 27.47 kW when the load is 20.4 Ω, which fulfills the Class 3 power standard of SAE [28].

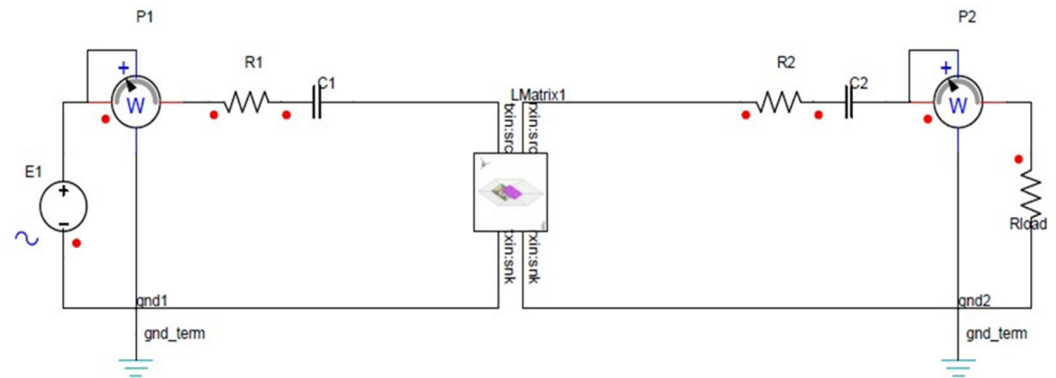


Figure 6. Simplorer circuit design.

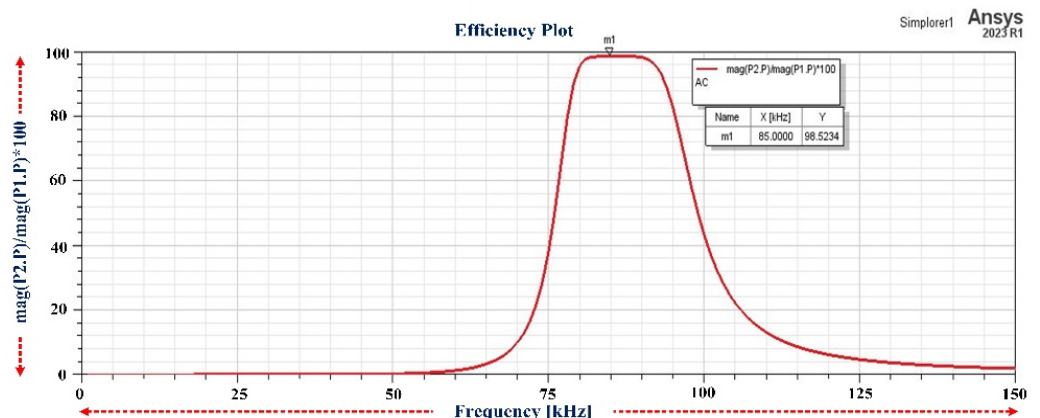


Figure 7. Efficiency vs. frequency.

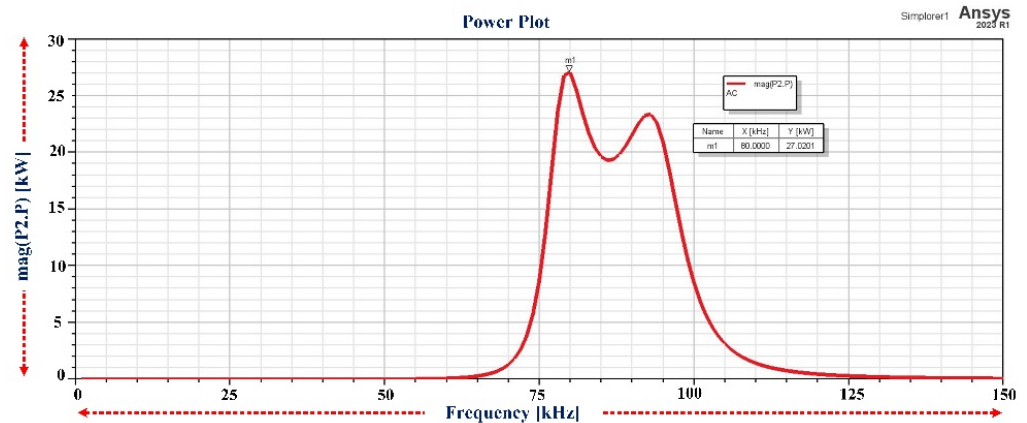


Figure 8. Output power vs. frequency.

The misalignment shown in Figure 9 and the data shown in Table 2 and Figure 10 are in accordance with the design described in Section 2.2. Figure 9 depicts the misalignment at X = 150 mm and Y = 150 mm, and Figure 10 shows the relation between efficiency and horizontal misalignment position. From Table 2, the efficiency is 98.52% when perfectly aligned, and it drops down to 5.61% at alignments of X = 150 mm and Y = 150 mm. Additionally, for the same alignment cases, the coupling coefficient’s value drops from 0.2168 to 0.0523.

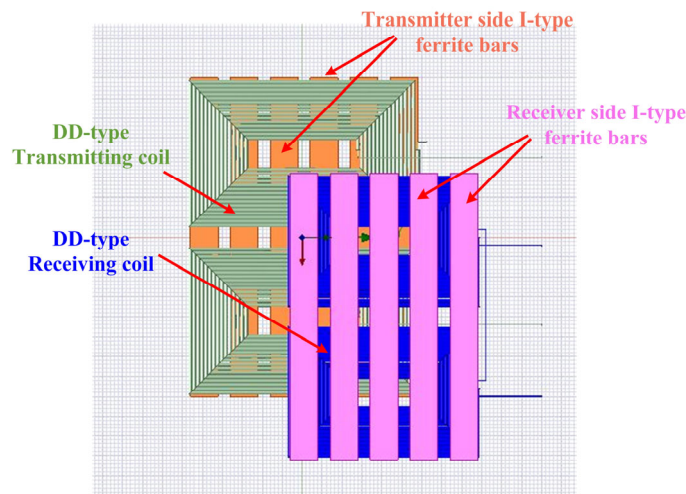


Figure 9. Horizontal misalignment (alignment: X = 150 mm, Y = 150 mm).

Table 2. Maximum coupling coefficient and efficiency at various horizontal misalignment positions.

Position	Horizontal Alignment	Coupling Coefficient (k_m)	Maximum Efficiency (%)
1	X = 0 mm, Y = 0 mm	0.2168	98.52
2	X = 0 mm, Y = 75 mm	0.1988	84.29
3	X = 75 mm, Y = 0 mm	0.1690	61.22
4	X = 75 mm, Y = 75 mm	0.1572	52.81
5	X = 0 mm, Y = 150 mm	0.1541	50.68
6	X = 150 mm, Y = 0 mm	0.0641	8.81
7	X = 150 mm, Y = 150 mm	0.0523	5.61

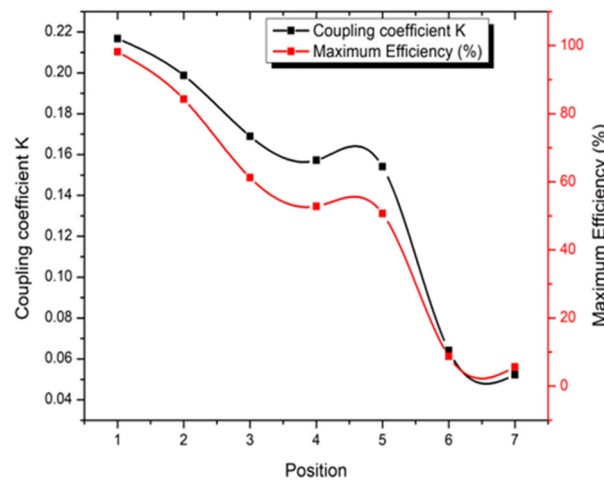


Figure 10. Plot between horizontal misalignment position vs. coupling coefficient K and efficiency.

Figure 11 describes that as the vertical distance increases between Tx and Rx coils, the coupling coefficient decreases and also results in a decrement in efficiency.

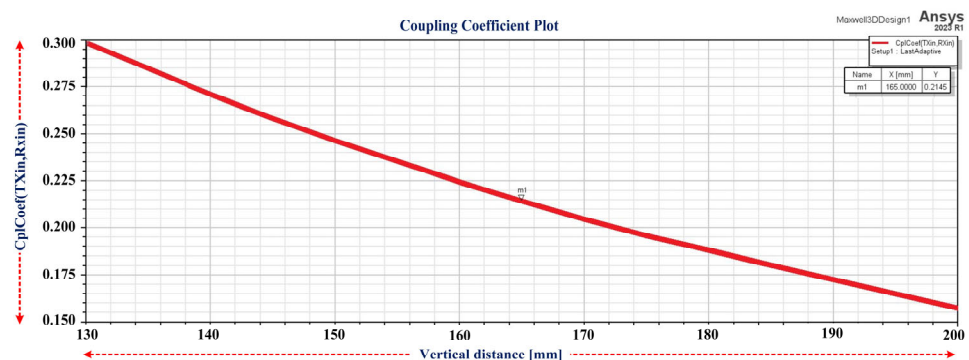


Figure 11. Plot between vertical distance vs. coupling coefficient k.

3.2. Optimization of Ferrite Core Dimensions

Optimizing ferrite core size in wireless charging systems for EVs is critical for efficiency and reliability. Researchers have given insight into amorphous magnetic material [29] and nanocrystalline ribbons [30], which can be preferred for advancement in WC technology in EVs. However, the inclusion of these materials should be aligned with a tradeoff between specific application needs and cost constraints. Moreover, proper dimensions improve coupling coefficients and ensure efficient energy transmission. Optimization helps with resonance tuning and matching with system needs. It improves alignment tolerance and compensates for misalignments in real-world circumstances. Considerations concerning size and weight are critical for their incorporation into electric cars. Overall, optimizing the size of ferrite cores is critical for satisfying requirements, improving performance, and ensuring the smooth and effective functioning of wireless charging systems. The optimization of I-type ferrite structures for inductively coupled wireless charging addresses the structure’s coupling performance while considering the three cases of total ferrite length and width.

3.2.1. Case 1: Constant Ferrite Width: 52.5 mm

As shown in Figure 4, the core lengths are progressively increased along the X-direction. The plot between the ferrite cores’ length and the coupling coefficient is shown in Figure 12. On the Rx, a peak value of 0.2283 is achieved with core lengths of 425 mm, while on the Tx, the peak value is 0.2258 with core lengths of 400 mm. However, from Table 3, it is evident

that the best-achieved k is 0.2418 at a fixed width of 52.5 mm and an effective length of 400 mm.

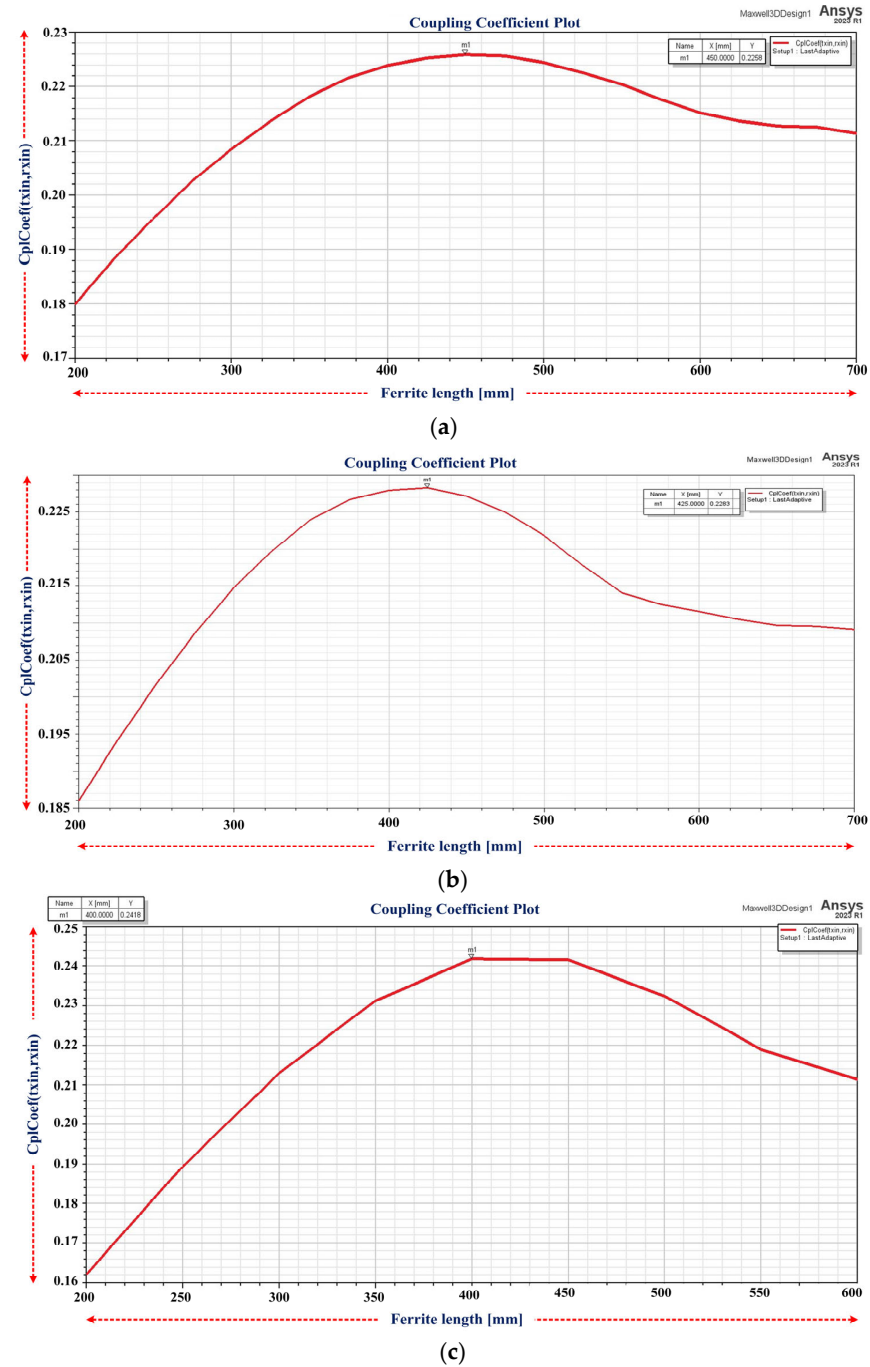


Figure 12. Plot between the length of the ferrite cores and the coupling coefficient (k): (a) Tx side only; (b) Rx side only; (c) both Tx and Rx side.

Table 3. Maximum coupling coefficient at optimum ferrite length.

Ferrite Length Varied at	Optimum Ferrite Length	Maximum Coupling Coefficient (k_m)
Transmitter side	450 mm	0.2258
Receiver side	425 mm	0.2283
Both sides	400 mm	0.2418

3.2.2. Case 2: Constant Ferrite Length at the Transmitter and Receiver Sides Is 600 mm and 540 mm, Respectively

In this case, the core length and width varied simultaneously in the X and Y directions. As indicated in Table 4, on the Rx, a peak value of 0.2195 is achieved with a core width of 52.5 mm, while on Tx side, the peak value is 0.2169 with a core width of 60 mm. However, from Table 4 and Figure 13, the peak value of k , 0.2178, is achieved when varying the ferrite width on both sides at the optimal width of 60 mm.

Table 4. Maximum coupling coefficient at optimum ferrite width.

Ferrite Width Varied at	Optimum Ferrite Width	Maximum Coupling Coefficient (k_m)
Transmitter side	60 mm	0.2169
Receiver side	52.5 mm	0.2195
Both sides	60 mm	0.2178

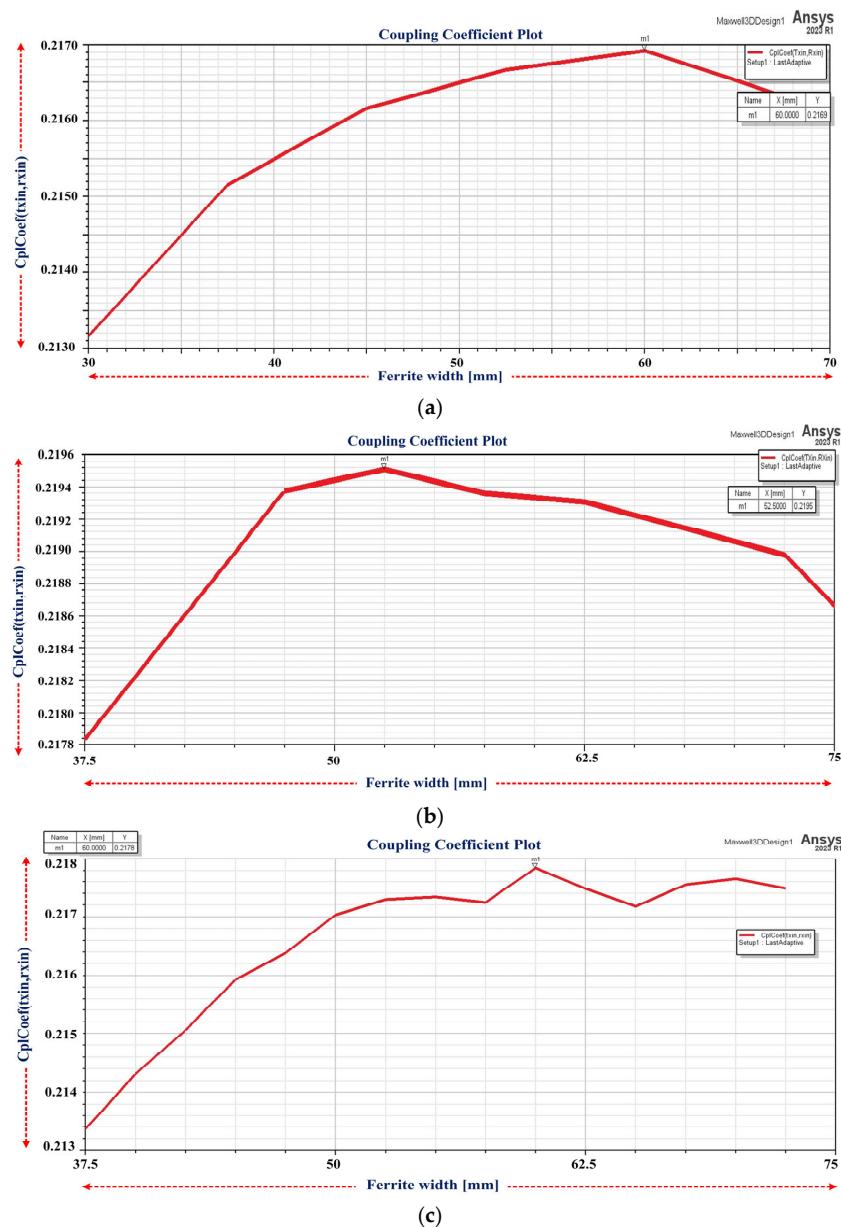


Figure 13. Plot between width of the ferrite cores and coupling coefficient k : (a) Tx side only; (b) Rx side only; (c) both Tx and Rx side.

3.2.3. Case 3: Ferrite Length and Width Vary Simultaneously

In this case, core length and width varied simultaneously in the X and Y directions. As indicated in Table 5, on the Rx, a peak value of 0.2260 is achieved with a core length and width of 500 mm and 67.5 mm, respectively, while on the Tx side, the peak value is 0.2320 with a core length and width of 400 mm and 67.5 mm, respectively. However, from Figure 14, it is evident that the peak value of k, 0.2451, is achieved when varying the ferrite length and width on both sides at the optimal length and width of 400 mm and 57.5 mm, respectively.

Table 5. Maximum coupling coefficient at optimum ferrite length and width.

Ferrite Length and Width Varied at	Optimum Ferrite Length and Width	Maximum Coupling Coefficient (k_m)
Transmitter side	500 mm and 67.5 mm	0.2260
Receiver side	400 mm and 67.5 mm	0.2320
Both sides	400 mm and 57.5 mm	0.2451

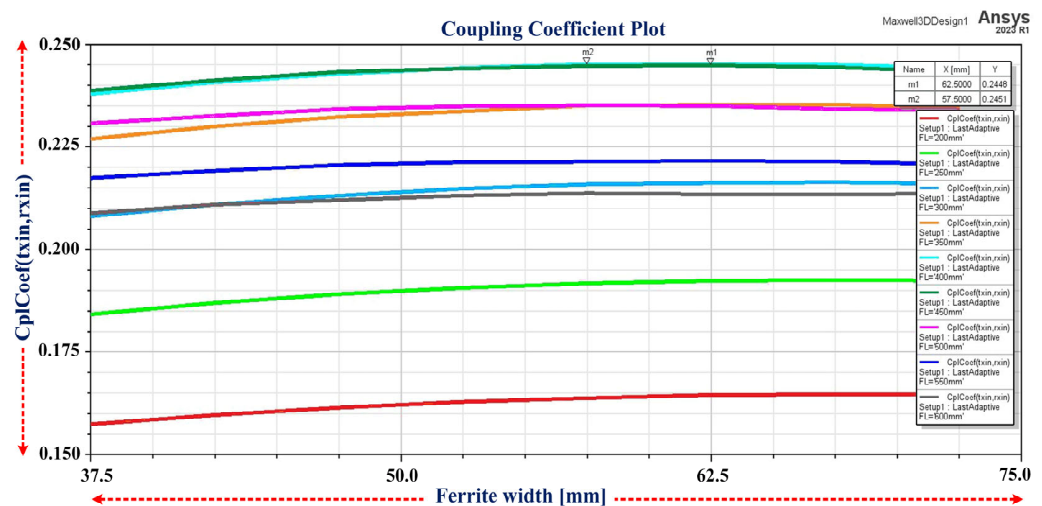


Figure 14. Ferrite cores versus coupling coefficient (k) when length and width are varied on Tx, Rx.

Figure 15 describes the design parameters of Tx and Rx to obtain optimality. It depicts about three cases, which correspond to the ferrite length, ferrite width, and coupling coefficient. From this figure, it is evident that the optimal k of 0.2451 is achieved while changing the length and width of ferrite on Tx and Rx. For this k value, the optimized length of each ferrite bar is 400 mm and its width is 57.5 mm. Further, the exact coupling coefficient is achievable with ferrite bars, and it depends on various factors including the specific design of the WCS, the quality of the ferrite material, and the distance between the coils. Moreover, it is important to note that a coupling coefficient above 0.2 is easily achievable, especially in the case of ferrite bars and, in some cases, substantially higher.

The above results provide a neat connection between ferrite core size, coupling coefficients, and the efficiency of ICWCS for electric vehicles. Moreover, these results are valid under the International Commission on Non-Ionizing Radiation Protection (ICNIRP) guidelines [31]. Thus, they contribute valuable insights to the ongoing efforts to optimize wireless charging systems. Consequently, this research paves the way for the widespread adoption of EVs in a sustainable and user-friendly manner. However, the proximity of the discussion in this work is limited to coil structure; there are other factors that play a crucial role in designing a system employing these coil structures.

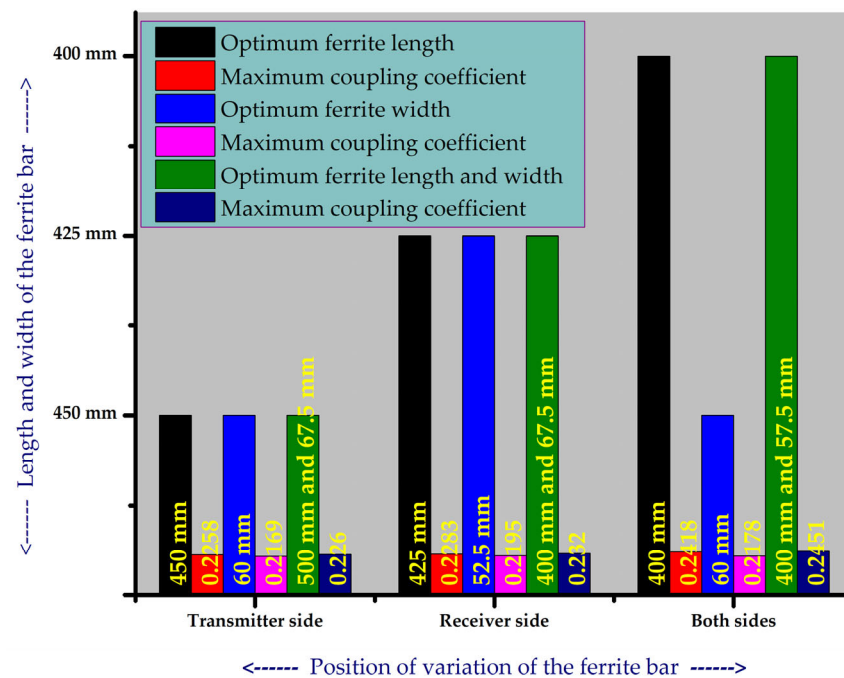


Figure 15. Dimension of ferrite bars versus their positional variation on Tx, Rx.

4. Conclusions

In this study, six I-type ferrite bars on the transmitter side and five I-type ferrite bars on the receiver side are constructed and simulated. There are two significant results. Firstly, 98.52% efficacy is achieved in the case of perfect alignment, while in the case of lateral and longitudinal misalignments of 150 mm, the efficacy drops to 5.61%. Further, the coupling coefficient's value drops from 0.2168 to 0.0523 for the same misalignment cases. Secondly, optimization of the I-type ferrite structures for inductively coupled wireless charging addresses the structure's coupling performance while considering the three cases of total ferrite length and width. The maximum obtained value of the coupling coefficient at the respective optimal ferrite dimensions is

1. 0.2418 at 400 mm of ferrite length when varied on both sides, keeping the width invariable at 52.5 mm;
2. 0.2195 at 52.5 mm of ferrite width when varied on the Rx side, keeping the length of 600 mm on the Tx side and of 540 mm on the Rx side;
3. 0.2451 at 400 mm of ferrite length and 57.5 mm of ferrite width when ferrite length and width are varied on both sides.

The above-mentioned results are based on the fact that optimal ferrite dimensions are required for the maximum coupling coefficient despite structural changes. As the ferrite dimensions increase, the mutual inductance increases, but the coupling coefficient decreases. Since the efficiency is directly proportional to the coupling coefficient, to achieve the maximum efficiency, the coupling coefficient must be maintained at its optimum value. The proposed system attained the highest coupling coefficient of 0.2451 at the optimal length and width of 400 mm and 57.5 mm, respectively, while varying ferrite length and width on both sides. Also, as per the ICNIRP guidelines, the obtained magnetic field density of the proposed coil structure is within the limits. Therefore, the obtained results can be implemented practically in the case of DD coils.

Author Contributions: Conceptualization and methodology, V.C.; validation, V.L.N.K.; formal analysis, V.C.; investigation V.L.N.K.; resources, V.L.N.K.; data curation, V.C.; writing—original draft preparation, V.C.; writing—review and editing, V.C.; visualization, V.C.; supervision, V.L.N.K.; All authors have read and agreed to the published version of the manuscript.

Funding: This research received no external funding.

Data Availability Statement: Data are contained within the article.

Acknowledgments: The authors would like to thank the Vellore Institute of Technology, Vellore, India, for their assistance in the completion of this work.

Conflicts of Interest: The authors declare no conflicts of interest.

Abbreviations

AC	Alternating current
DC	Direct current
EV	Electric vehicle
WC	Wireless charging
WCS	Wireless charging system
DWCS	Dynamic wireless charging system
ICWCS	Inductively coupled wireless charging system
DD	Double-D
3D	Three-dimensional
FEM	Finite element technique
SAE	Society of Automotive Engineers
HFT	High frequency transformer
IPT	Inductive power transfer
WPT	Wireless power transfer
Tx	Transmitting coil
Rx	Receiving coil
M	Mutual inductance
k	Coupling coefficient
L_T	Self-inductance of Tx
L_R	Self-inductance of Rx
C_T	Capacitance of Tx
C_R	Capacitance of Rx
R_T	Resistance of Tx
R_R	Resistance of Rx
R_L	Load resistance
ICNIRP	International Commission on Non-Ionizing Radiation Protection
k_m	Maximum coupling coefficient

References

1. Catrysse, M.; Hermans, B.; Puers, R. An inductive power system with integrated bi-directional data-transmission. *Sens. Actuators A Phys.* **2004**, *115*, 221–229. [CrossRef]
2. Mathesh, G.; Saravanakumar, R. A Novel Intelligent Controller-Based Power Management System with Instantaneous Reference Current in Hybrid Energy-Fed Electric Vehicle. *IEEE Access* **2023**, *11*, 137849–137865. [CrossRef]
3. Mohamed, A.A.S.; Shaier, A.A.; Metwally, H.; Selem, S.I. An Overview of Dynamic Inductive Charging for Electric Vehicles. *Energies* **2022**, *15*, 5613. [CrossRef]
4. Vaka, R.; Keshri, R.K. Design considerations for enhanced coupling coefficient and misalignment tolerance using asymmetrical circular coils for WPT system. *Arab. J. Sci. Eng.* **2019**, *44*, 1949–1959. [CrossRef]
5. Bouanou, T.; Fadil, H.E.; Lassioui, A.; Bentalhik, I.; Koundi, M.; Jeilani, E.S. Design Methodology and Circuit Analysis of Wireless Power Transfer Systems Applied to Electric Vehicles Wireless Chargers. *World Electr. Veh. J.* **2023**, *14*, 117. [CrossRef]
6. Chakibanda, V.; Komanapalli, V.L. Optimization in Magnetic Coupler Design for Inductively Coupled Wireless Charging of Electric Vehicle: A Review. *Arab. J. Sci. Eng.* **2023**, *48*, 14257–14294. [CrossRef]
7. Economic and Environmental Sustainability of Dynamic Wireless Power Transfer for Electric Vehicles Supporting Reduction of Local Air Pollutant Emissions—ScienceDirect. Available online: <https://www.sciencedirect.com/science/article/pii/S1364032120308212> (accessed on 7 July 2023).
8. Ushijima-Mwesigwa, H.; Khan, M.Z.; Chowdhury, M.A.; Safro, I. Optimal installation for electric vehicle wireless charging lanes. *arXiv* **2017**, arXiv:1704.01022.
9. Bandyopadhyay, S.; Venugopal, P.; Dong, J.; Bauer, P. Comparison of magnetic couplers for ipt-based EV charging using multi-objective optimization. *IEEE Trans. Veh. Technol.* **2019**, *68*, 5416–5429. [CrossRef]

10. Kadem, K.; Bensetti, M.; Le Bihan, Y.; Labouré, E.; Debbou, M. Optimal Coupler Topology for Dynamic Wireless Power Transfer for Electric Vehicle. *Energies* **2021**, *14*, 3983. [\[CrossRef\]](#)
11. Budhia, M.; Covic, G.; Boys, J. A new IPT magnetic coupler for electric vehicle charging systems. In Proceedings of the IECON 2010—36th Annual Conference on IEEE Industrial Electronics Society, Glendale, AZ, USA, 7–10 November 2010; pp. 2487–2492.
12. Cheng, Y.; Shu, Y. A new analytical calculation of the mutual inductance of the coaxial spiral rectangular coils. *IEEE Trans. Magn.* **2014**, *50*, 7026806. [\[CrossRef\]](#)
13. Aissaoui, M.; Allag, H.; Yonnet, J.P. Mutual inductance and interaction calculation between conductor or coil of rectangular cross section and parallel piped permanent magnet. *IEEE Trans. Magn.* **2014**, *50*, 7027704. [\[CrossRef\]](#)
14. Smeets, J.P.C.; Overboom, T.T.; Jansen, J.W.; Lomonova, E.A. Three-dimensional magnetic field modeling for coupling calculation between air-cored rectangular coils. *IEEE Trans. Magn.* **2011**, *47*, 2935–2938. [\[CrossRef\]](#)
15. Kushwaha, B.K.; Rituraj, G.; Kumar, P. 3d analytical model for computation of mutual inductance for different misalignments with shielding in wireless power transfer system. *IEEE Trans. Transp. Electrification* **2017**, *3*, 332–342. [\[CrossRef\]](#)
16. Joy, E.; Dalal, A.; Kumar, P. Accurate computation of mutual inductance of two air core square coils with lateral and angular misalignments in a flat planar surface. *IEEE Trans. Magn.* **2014**, *50*, 7000209. [\[CrossRef\]](#)
17. Yang, Z.; Chen, Y.; Yang, D.; Du, W.; He, G.; Zhang, X.; Xu, C.; Wang, W. Research on parameter optimization of Double-D coils for electric vehicle wireless charging based on magnetic circuit analysis. *IEICE Electron. Express* **2020**, *17*, 20200067. [\[CrossRef\]](#)
18. Hassanein, W.; Enany, M.A.; Shaier, A.A.; Ahmed, A.A. Performance analysis of rectangular and double-D transmitters with various receivers for electric vehicle static charging. *Alex. Eng. J.* **2023**, *78*, 438–452. [\[CrossRef\]](#)
19. Yang, Y.; Cui, J.; Cui, X. Design and Analysis of Magnetic Coils for Optimizing the Coupling Coefficient in an Electric Vehicle Wireless Power Transfer System. *Energies* **2020**, *13*, 4143. [\[CrossRef\]](#)
20. Chi, F.; Wang, P.; Sun, C.; Wu, Y.; Dou, Z.; Xu, C.; Wang, S.; Wang, W. Research on Optimization of Horizontal Omnidirectional Misalignment Tolerance of WPT Based on Double D Coupler. *Electronics* **2022**, *11*, 2163. [\[CrossRef\]](#)
21. Bensetti, M.; Kadem, K.; Pei, Y.; Le Bihan, Y.; Labouré, E.; Pichon, L. Parametric Optimization of Ferrite Structure Used for Dynamic Wireless Power Transfer for 3 kW Electric Vehicle. *Energies* **2023**, *16*, 5439. [\[CrossRef\]](#)
22. Choi, B.-G.; Kim, Y.-S. New Structure Design of Ferrite Cores for Wireless Electric Vehicle Charging by Machine Learning. *IEEE Trans. Ind. Electron.* **2021**, *68*, 12162–12172. [\[CrossRef\]](#)
23. Luo, Z.; Wei, X.; Pearce, M.G.S.; Covic, G.A. Multiobjective optimization of inductive power transfer double-D pads for electric vehicles. *IEEE Trans. Power Electron.* **2020**, *36*, 5135–5146. [\[CrossRef\]](#)
24. Mohammad, M.; Choi, S. Optimization of ferrite core to reduce the core loss in double-D pad of wireless charging system for electric vehicles. In Proceedings of the 2018 IEEE Applied Power Electronics Conference and Exposition (APEC), San Antonio, TX, USA, 4–8 March 2018; pp. 1350–1356.
25. Gu, B.S.; Dharmakeerthi, T.; Kim, S.; O’Sullivan, M.J.; Covic, G.A. Optimised Magnetic Core Layer in Inductive Power Transfer Pad for Electric Vehicle Charging. *IEEE Trans. Power Electron.* **2023**, *38*, 11964–11973. [\[CrossRef\]](#)
26. Bosshard, R.; Iruretagoyena, U.; Kolar, J.W. Comprehensive evaluation of rectangular and double-D coil geometry for 50 kW/85 kHz IPT system. *IEEE J. Emerg. Sel. Top. Power Electron.* **2016**, *4*, 1406–1415. [\[CrossRef\]](#)
27. Shaier, A.A.; Mohamed, A.A.; Metwally, H.; Selem, S.I. New design of high-power in-motion inductive charger for low power pulsation. *Sci. Rep.* **2023**, *13*, 17838. [\[CrossRef\]](#) [\[PubMed\]](#)
28. SAE TIR J2954_201605; Wireless Power Transfer for Light-Duty Plug-in/Electric Vehicle and Alignment Methodology. SAE International: Warrendale, PA, USA, 2016.
29. Luo, Z.; Li, X.; Jiang, C.; Li, Z.; Long, T. Permeability-adjustable nanocrystalline flake ribbon in customized high-frequency magnetic components. *IEEE Trans. Power Electron.* **2023**, *39*, 3477–3485. [\[CrossRef\]](#)
30. Ou, J.; Liu, Y.; Breining, P.; Schiefer, M.; Doppelbauer, M. Experimental study of the amorphous magnetic material for high-speed sleeve-free PM rotor application. *IEEE Trans. Ind. Electron.* **2019**, *67*, 4422–4432. [\[CrossRef\]](#)
31. International Commission on Non-Ionizing Radiation Protection. Guidelines for limiting exposure to time-varying electric and magnetic fields (1 Hz to 100 kHz). *Health Phys.* **2010**, *99*, 818–836. [\[CrossRef\]](#)

Disclaimer/Publisher’s Note: The statements, opinions and data contained in all publications are solely those of the individual author(s) and contributor(s) and not of MDPI and/or the editor(s). MDPI and/or the editor(s) disclaim responsibility for any injury to people or property resulting from any ideas, methods, instructions or products referred to in the content.